Mechanics of hydraulic fracturing in ultra-low permeability formations: role of cavitation and sorption

Sandeep Kumar, Matias Zielonka, Kevin Searles, Ganesh Dasari
ExxonMobil Upstream Research Company
22777 Springwoods Village Parkway
Spring, Texas 77389

Abstract

Hydraulic fracturing (HF) comprises nucleation and growth of fractures in rock formations via flow-induced pressurization. HF is routinely used as a means of stimulating low permeability rock formations to enhance the recovery of oil and gas. The physical processes in the fracture process zone (FPZ) during HF are usually very complex because of the coupling between fracturing-fluid flow, rock deformation and diffusion of host fluid. Identifying all the critical pieces of physics is the key to developing a reliable full-physics modeling and simulation capability. Such a capability will not only enhance our understanding of HF but will also aid greatly towards the development of an effective stimulation strategy. The role of cavitation and sorption is typically ignored in hydraulic fracturing simulations because the rock formations are believed to remain always fully saturated during HF. However, by combining the multi-physics Finite Element Analysis (FEA) with the analysis of Polyaxial Test Cell (PTC) experiments, we show that ignoring cavitation and sorption leads to spurious outcomes in the FEA simulations of fluid-driven fractures in low permeability formations. The FEA simulations, in the absence of cavitation and sorption, predict an unrealistically large suction (negative pressure) ahead of the crack tip which grows without bound upon refinement of the FEA mesh. Because of such a large suction at the crack tip, the breakdown pressure obtained from the simulations is anomalously large and lacks objectivity (i.e., progressively increases upon a continued refinement of the FEA mesh). Mechanistic insights gained form FEA simulations suggest that the negative pressure ahead of the crack tip causes cavitation, resulting in the creation of a partially-saturated region around the crack tip. This means that irrespective of the initial saturation of the rock, inclusion of cavitation and sorption phenomena in the modeling is necessary for adequately resolving the physical processes in the FPZ. The revised FEA simulations of hydraulic fracturing show that the inclusion of cavitation and sorption in the simulations eliminates the unrealistically large suction at the crack tip, regularizes the breakdown pressure and removes the noted lack of objectivity.

Keywords: hydraulic fracturing, soil mechanics, cohesive elements, cavitation, sorption.

1 Introduction

Hydraulic fracturing involves opening and propagation of a crack inside a rock by means of pressure induced by fluid flow. Hydraulic fracturing is of great technological importance in the oil and gas industry since it constitutes a key component of a number of important field operations. Key examples include (a) stimulation of formations with ultra-low permeability such as shale, where the main purpose is to enhance the recovery of hydrocarbons from low permeability formations such as sandstones and shale rocks, (b) Produced Water Re-Injection (PWRI), where the produced water is injected into the formation to fill the space created by produced hydrocarbons, and (c) Cutting Re-Injection (CRI) in which slurry from drill cuttings is disposed in the subsurface via re-injection. In each of these applications, hydraulic fracturing enhances the operational effectiveness by creating new surfaces in the rock via fracturing and hence increases the surface area through which the fluid can diffuse from or to the interior of the rock.

Operationally, the process of hydraulic fracturing comprises injecting a fracturing fluid into a confined space in the interior of a formation, as schematically shown in Fig.[1]. During injection, both the fluid pressure and the volume of the injected fluid are recorded as a function of time. Prior to the onset of fracture propagation, the injection-pressure monotonically increases until it reaches a value that is high enough to initiate a fracture.

Once such value is reached, the pressure generated by the fluid eventually opens up a crack which subsequently propagates through the matrix. The fracture propagation corresponds to the peak in the pressure-response curve. Once the crack has been propagated to a sufficiently long length, the flow is shut down. Consequently, a pressure drop corresponding to fracture closure is recorded in the measured response.

Knowledge of the correlation between treating pressure and geometry of the resulting fracture is the key to economical design of hydraulic fracturing field operations. However, such correlations are not unique and vary both with the local rock conditions (strength, permeability, and saturation level) as well as with the fracturing fluid properties (viscosity, density etc.) One way to develop such correlations is via measuring fracture geometry and pressure response for a number of trial cases. However, the *in-situ* measurement of fracture geometry in HF still remains beyond the scope of current capabilities due to enormous difficulties with performing experiments in the interior of the earth, where the fracturing process takes place. For this reason, reliable methods of determining fracture geometries in hydraulic fracturing are currently lacking. Some insights into the process of hydraulic fracturing can be gained by Polyaxial Test Cell (PTC) experiments (El Rabaa 1987), which allow studying fracturing of geological rocks by means of hydraulically induced pressure at laboratory scale. However, properly scaling up the results of such laboratory level experiments to the field level poses significant difficulties, severely limiting the usability of such experiments. Moreover, in such experiments, the region ahead of the crack tip remains inaccessible to observation, presenting difficulties in probing the physical processes that take place in the crack tip region. For this reason, a multi-physics simulation capability becomes inevitably required for predicting fracture geometries in hydraulic fracturing. Moreover, such simulations also allow access to the mechanistic processes taking place in the crack tip region which are otherwise inaccessible to physical observations and measurements.

Computational modeling and simulation, if underpinned with all necessary physics, can provide a reliable prediction of fracture geometry as well as a detailed insight into the physical processes occurring in the crack tip region. However, computational modeling of HF is fraught with enormous difficulties. The difficulties originate primarily from the coupling between the complex physical processes involved in hydraulic fracturing, such as (1) the flow of the fracturing fluid within the fracture, (2) the flow of the pore fluid and seepage of fracturing fluid within the pores, (3) the deformation of a porous medium induced by both the hydraulic pressurization of the fracture and the compression/expansion and transport of pore fluid within the pores, and (4) the fracture propagation via subsequent damage of the material. Most of the currently existing commercial hydraulic fracture simulators used in the oil and natural gas industry rely on simplified models where some of the couplings between the various physical processes are simplified. Consequently, the applicability and accuracy of these simulators is limited to oversimplified scenarios, and a reliable prediction of fracture geometry and pressure response under realistic geologies, wellbore configurations and in-situ stress conditions remains beyond the scope of such simulators.

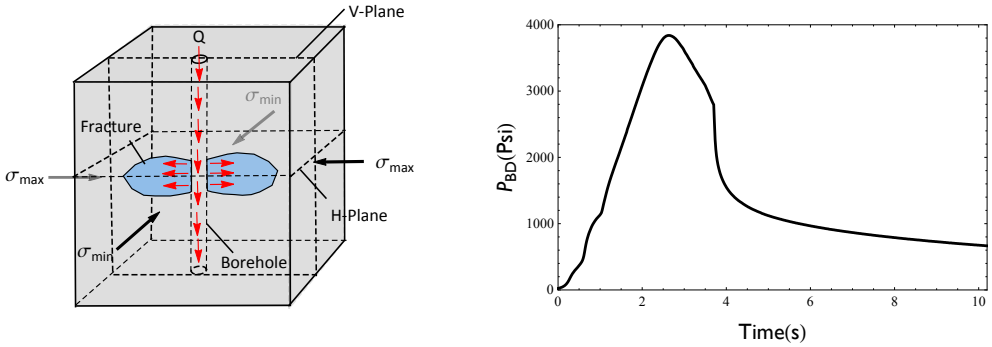

Figure 1: (a) A schematic illustration of the process of hydraulic fracturing. Fracture is initiated by injecting a fracturing fluid into a hydrostone matrix. By combining different choices for fracturing fluid and hydrostone matrix, a wide range of hydraulic conductivity scenarios can be realized. Fracture growth occurs normal to the direction of minimum confining stress, and the resulting fracture is typically bi-winged in geometry. (b) Shown is a typical injection pressure versus time curve obtained from a PTC experiment. The peak value is called breakdown pressure and corresponds to the point beyond which the fracture steadily propagates.

ExxonMobil Upstream Research Company and Dassault Systemes Simulia Corporation recently co-developed a

fully-coupled hydraulic fracturing simulation capability which combines the nonlinear soil consolidation analysis with newly developed coupled pressure/deformation cohesive elements (`COD2D4P` in 2D and `COD3D8P` in 3D) (see Zielonka et al 2014, Ning et al 2015). These elements allow modeling of progressive damage of mechanical strength as well as the flow of the fracturing fluid within the fracture. This new capability rigorously incorporates many of the essential physics which were previously ignored in most of the commercial hydraulic fracturing simulators.

Diffusion of the host fluid through the matrix in response to an ongoing deformation is a distinguishing aspect of hydraulic fracturing. One of the factors governing stress-driven fluid diffusion in a rock is the absolute permeability (k_a) of the rock, which basically characterizes how well the pores in the rocks are connected. The absolute permeability may greatly vary depending upon both the nature of the rock formation as well as its state of consolidation (Zoback 2007). For example, a typical sandstone has a permeability of the order of 10 miliDarcy (mD) whereas a typical shale has a permeability of the order of nanoDarcy (nD). From a production point of view, a formation with higher permeability is desirable. However, a higher permeability alone is not sufficient to ensure an unrestricted flow of a fluid through a rock. For example, the pores in the rock may be well-connected, but the mobility of the fluid may be still impacted by an intrinsic viscous resistance to fluid flow. The mobility of a fluid through a solid should be a joint fluid-solid property. This is a consequence of Darcy's law, which relates the fluid flux through the material to the applied pressure-difference:

$$\dot{\zeta} = \frac{k_a \rho g}{\mu} \nabla p, \tag{1}$$

where $\dot{\zeta}$ is the fluid weight flowing through per unit cross-section per unit time, k_a is the absolute permeability of the rock, ρ is the density of the fluid, g is the acceleration due to gravity, μ is the dynamic viscosity of the fluid, and ∇p is the pressure gradient. Thus, according to Darcy's law, the flow rate induced in response to an applied pressure-difference is determined not only by the absolute permeability of the solid, but also by the viscosity of the fluid. Therefore, the poroelastic response of the material is often described by a joint property of the solid-fluid system, called hydraulic conductivity. The hydraulic conductivity of a rock formation saturated with a given fluid is given by:

$$k_{\text{Fluid}} = \frac{k_a \rho g}{\mu}, \tag{2}$$

and it governs the movement of the fluid through the pores of the solid.

Depending upon the viscosity and density of the host fluid, a given formation can have very different values of hydraulic conductivity, as shown in Fig [2]. For example, shale formations have an ultra-low absolute permeability, typically of the order of nD. Such a formation, when the host fluid is a gas, would have a hydraulic conductivity of $k_{\text{Fluid}} = 1 \times 10^{-9}$ in/s. The same formation, when saturated with a light oil, would have a hydraulic conductivity of $k_{\text{Fluid}} = 1 \times 10^{-11}$ in/s. Because of such wide variation in hydraulic conductivity of rock formations, it is necessary to ensure that the computational model is able to provide adequate solution for the entire breadth of hydraulic conductivity spectrum.

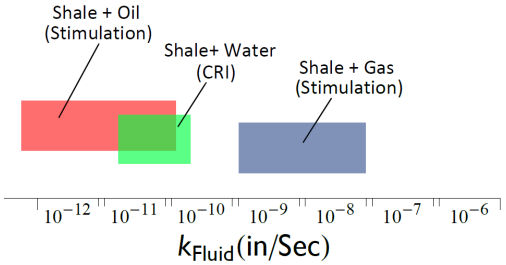

Figure 2: Hydraulic conductivity values of a shale formation for different host fluids.

One of the main challenges associated with computational modeling is to ensure the sufficiency of physics in the underlying model. Typically, in poroelastic solids, a mechanical deformation is followed by an adjustment in pore pressure due to flow of the host fluid between pores. Such adjustment prevents build-up of large gradients in pore pressure within the material. The fluid flow between the pores, as discussed previously, is predominantly Darcy

flow and is mainly limited by the hydraulic conductivity of the solid-fluid system. The formations with ultra-low permeability constitute a special case in this regard since in such formations, the adjustment of pore pressure due to Darcy flow would be very minimal. In the absence of such adjustment, a large dilatational deformation of the material, which is common during HF, could cause large negative pressures in the material. Certainly, a fluid cannot sustain a large negative pressure and therefore, in reality, a negative pressure would entail other physical mechanisms such as cavitation that would eventually renormalize the pore-pressure in the material. For adequately modeling hydraulic fracturing in ultra-low permeability formations, the description of such physical mechanisms should be included the underlying model.

The main objective of this work is to investigate if the co-developed multi-physics simulation capability is sufficiently enabled, i.e., it contains all the necessary physics to adequately model hydraulic fracturing in ultra-low permeability formations such as shale. In Sec.(2), we have summarized the governing equations and the constitutive relations describing the various physical processes associated with hydraulic fracture modeling. Sec.(3) focuses primarily on objectivity of FEA simulations for the range of hydraulic conductivities illustrated in Fig. 2. The purpose of the objectivity analysis is to establish if the FEA models contain all the necessary physics required to model the hydraulic fracturing process and whether the FEA solutions are insensitive to the FEA mesh employed. It will be noted that such objectivity is lacking for ultra-low permeability formations. In Sec.(4), we show that the noted lack of objectivity originates from the absence of cavitation and sorption physics in the FEA model, and consequently, we suggest a resolution to this anomaly by inclusion of such physics. The article is concluded in Sec.(5) with remarks on the implication of this work for stimulation in shale formations.

2 Governing Equations

The equations and constitutive relations governing the various physical processes associated with hydraulic fracturing are summarized below.

2.1 Elastic deformation of the matrix

The matrix is modeled as an isotropic, poroelastic material undergoing quasi-static deformation. The equation of equilibrium in terms of total stress tensor reads as:

$$\nabla.\boldsymbol{\sigma} = 0. \tag{3}$$

The total stress tensor relates to the effective stress tensor via the following relation (Terzaghi 1925):

$$\boldsymbol{\sigma} = \boldsymbol{\sigma}' + \alpha\, p\, \mathbf{I}, \tag{4}$$

where $\boldsymbol{\sigma}'$ is the effective stress tensor, α is Biot's coefficient, p is the pore pressure, and $\mathbf{I}$ is the identity matrix. The constitutive equation, relating effective stress tensor to strain tensor $\boldsymbol{\epsilon}$, reads as

$$\boldsymbol{\sigma}' = \lambda\, \mathrm{tr}\, \boldsymbol{\epsilon} + 2G\, \boldsymbol{\epsilon} - \alpha\, p\, \mathbf{I}, \tag{5}$$

where λ and G are Lamé constants.

2.2 Pore Fluid Flow

The continuity equation for the pore fluid reads as

$$\frac{1}{M}\, \dot{p} + \alpha\, \mathrm{tr}\, \dot{\boldsymbol{\epsilon}} + \nabla.\mathbf{v} = 0. \tag{6}$$

where $\mathbf{v}$ is the seepage velocity of the pore fluid, and M and α are Biot's modulus and Biot's coefficient, respectively. The seepage velocity $\mathbf{v}$ relates to the pressure-gradient ∇p via Darcy's law:

$$\mathbf{v} = -\frac{k_a}{\mu} \nabla p, \tag{7}$$

where k_a is the absolute permeability of the formation and μ is the dynamic viscosity of the pore fluid. Upon combining equation (6) and equation (7), the continuity equation becomes (Biot 1941, Biot 1955)

$$\frac{1}{M}\dot{p} + \alpha \,\mathrm{tr}\,\dot{\boldsymbol{\epsilon}} = \frac{k_a}{\mu}\nabla^2 p. \tag{8}$$

2.3 Fracturing fluid flow

Flow of the fracturing fluid within the fracture is described by lubrication theory. The governing equation reads as

$$\dot{g} + \frac{\partial q}{\partial l} + v_T + v_B = 0, \tag{9}$$

where g is the fracture gap, q is fracturing fluid flow (per unit width), and v_T and v_B are the normal flow velocities through the top and the bottom surfaces of the fracture. The fluid flow q relates to the pressure-difference along the fracture via the following relation:

$$q = -\frac{g^3}{12\mu_f}\frac{\partial p}{\partial l}, \tag{10}$$

where l is the curvilinear coordinate along the fracture, and μ_f is the dynamic viscosity of the fracturing fluid.

2.4 Fracture initiation and propagation

Fracture modeling in FEA simulations is treated within the framework of the Cohesive Zone Model (CZM)(Barenblatt 1959, Barenblatt 1962, Dugdale 1960). The key hypothesis in CZM is that the physical separation ahead of the crack tip occurs within a zone, called the cohesive zone, of length l_{cz}. The material separation within the cohesive zone is treated with the strength of material-based idea by means of a traction-separation (t-s) relation. A traction-separation relation is a functional relation between opening traction and fracture opening, and is an intrinsic material property. For the purpose of this study, we have employed a bilinear cohesive law, a schematic of which is shown in Fig.[3].

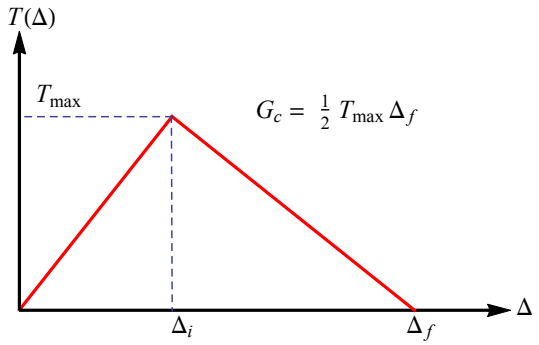

Figure 3: Bilinear traction-separation relation employed in this work.

The area under the traction-separation relation equals the fracture toughness G_c of the material. Δ_i is the separation at damage initiation while Δ_f denotes the separation at complete failure. The stress $T_{\max}$ at which the failure initiates is related to G_c and Δ_f as follows:

$$T_{\max} = \frac{2G_c}{\Delta_f}. \tag{11}$$

3 FEA Simulations

3.1 Geometry, boundary conditions and FEA discretization

The FEA simulations in this work are based on an analysis of PTC experiments, a schematic of which is shown in Fig.[1-a] (see Ning *et al.* 2015). That is, the geometry, boundary/loading conditions, and the matrix properties in

the FEA simulations correspond to that in the PTC experiments of Ning *et al.*. PTC experiments allow analyzing the process of hydraulic fracturing at a laboratory scale. Notably, in PTC experiments, the resulting fracture is strictly confined in a single plane (indicated as V-Plane in the schematic of Fig.[1]) and this permits simplifying the FEA model as a plane strain configuration (in H-plane) as shown in Fig.[4-a]. Further, since the fracture grows symmetrically on the two sides of the bore-hole, we employ a symmetry boundary condition along the bore-hole to reduce the simulation cell size. The domain is meshed using 2D plane strain quadrilateral elements with pore pressure degrees of freedom (`CPE4P`) while the crack seam is modeled using zero-thickness cohesive elements with pore pressure degrees of freedom (`COD2D4P`). A representative mesh is shown in Fig.(4-b). Fluid transmission into the cavity is carried out via special 2D pipe elements (`FP2D2`). The transmission of fluid pressure from the pipe to the borehole is modeled via a poromechanical loading.

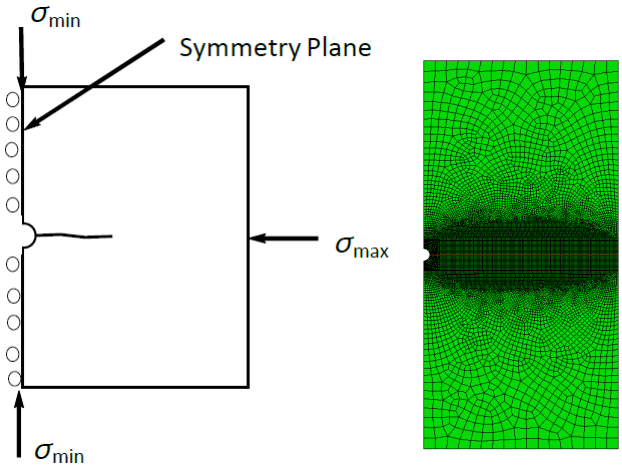

Figure 4: (a) Simulation domain and the boundary/loading condition used in the FEA simulations. (b) A respresentative FEA mesh used in this study. Shown in red is the cohesive crack seam modeled using zero thickness `COD2D4P` elements.

For the purpose of comparison, in this study we consider two formations with same mechanical properties (stiffness and strength) but very different hydraulic conductivities. The first formation, termed Formation A, has an ultra-low hydraulic conductivity $k_{\text{Fluid}} = 2.6 \times 10^{-12}$ in/s. Such a formation represents a shale rock which is saturated with oil. The second formation has a relatively higher hydraulic conductivity $k_{\text{Fluid}} = 2.6 \times 10^{-9}$ in/s and corresponds to a shale rock saturated with a gas. The poromechanical properties of the two formations are listed in Tab.[1].

	Formation A	**Formation B**
Elastic modulus	3.5×10^6 Psi	3.5×10^6 Psi
Poisson ratio	0.22	0.22
Permeability	0.28 mD	15 mD
Viscosity	3×10^4 cSt	1.5×10^3 cSt
Hydraulic conductivity	2.59×10^{-12} in/sec	2.59×10^{-9} in/sec
Tensile strength	1100 Psi	1100 Psi

Table 1: Summary of the poromechanical properties of the two formations considered in the FEA simulations. Both the matrix grains and the host fluid are considered incompressible so that the Biot coefficient is unity.

3.2 FEA results

3.2.1 Formation A : $k_{\mathbf{Fluid}} = \mathcal{O}(10^{-12}\mathbf{in/s})$

First, a configuration is analyzed in which the hydraulic conductivity of the host fluid with respect to the matrix is extremely low. Experimentally (see Ning *et al.* 2013), such a configuration is realized by combining the *Super-X* hydrostone matrix, which has an absolute permeability of $k_a = 0.28$ mD, with an extremely viscous fracturing fluid silicone oil, which has a kinematic viscosity of $\mu \sim 2.8 - 3.5 \times 10^4$ cSt. The resulting combination has an extremely low hydraulic conductivity: $k_{\text{Fluid}} = 2.5 \times 10^{-12}$ in/s. Because of such low hydraulic conductivity, this configuration is referred to as "*ultra-low permeability configuration*" in the rest of this documentation. Such a value of hydraulic conductivity is typical for geologic systems comprising a shale formation saturated with oil. Thus, the considered value remains relevant from a stimulation point of view.

FEA simulations are carried out with a progressively refined mesh. The injection pressure versus time curves obtained from these simulations are shown in Fig.[5-a]. Surprisingly, the breakdown pressure observed in FEA simulations monotonically increases as the characteristic element size in the FEA mesh decreases, and this is observed at all levels of mesh refinements (see Fig.[5-b]). The absence of mesh-size independence in a FEA simulation is known as lack of objectivity. One example of lack of objectivity is seen in linear elastic fracture mechanics where the stress field at the crack tip monotonically increases as the mesh in the crack tip region is progressively refined, and as a result, the apparent strength of the material is such simulations is subjective to FEA discretization (mesh size). The lack of objectivity is a serious issue from a numerical modeling point of view. Objectivity is the very first requirement for a FEA simulation to be meaningful since if it is not ensured, it will mean that the solution from the FEA simulation can be made arbitrarily large or small simply by varying the element-size in FEA mesh. A solution lacking objectivity does not correspond to any realistic material behavior.

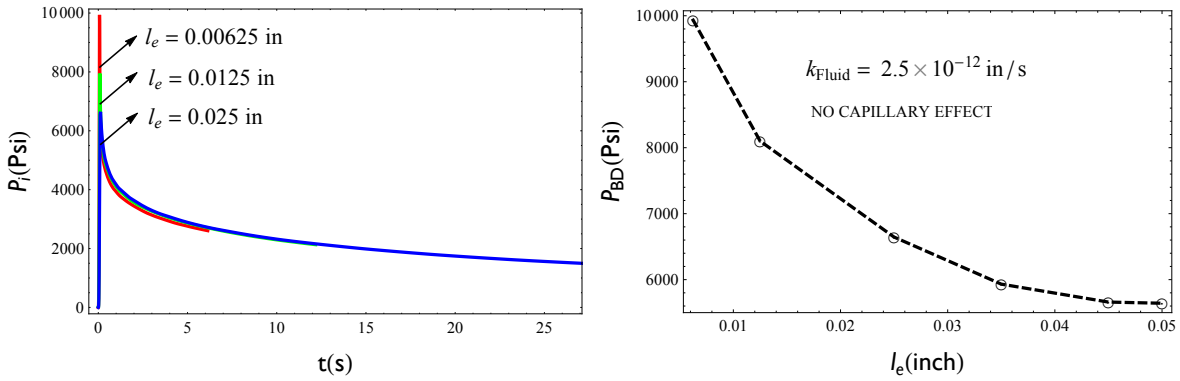

Figure 5: (a)Time history of injection pressure for progressive mesh refinement. Progressively sharper and higher peaks are obtained as the mesh is progressively refined. (b) Trend showing the variation in breakdown pressure with the element size.

The apparent strengthening of the matrix with mesh refinement in FEA simulations also has a corresponding impact on the crack geometry, as shown in Fig.(6). For example, the crack width progressively increases with mesh refinement whereas the crack length decreases upon mesh refinement. This variation in simulated fracture geometry can be understood by noting the fact that a higher peak means a larger area under the pressure versus time curve, which essentially translates into higher energy. This energy is invested into widening the crack, resulting in a wider crack for a higher peak.

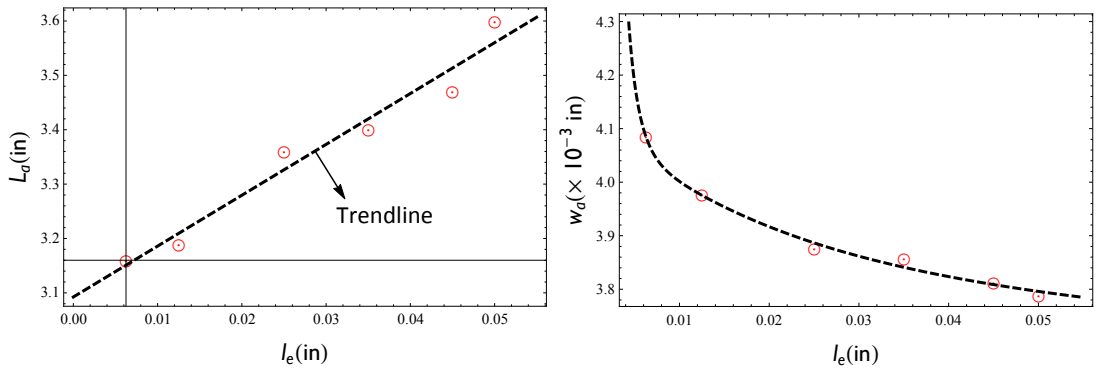

Figure 6: (a) Crack length at a fixed time instant obtained from the FEA simulations with progressively decreasing element size. (b) Crack width at a fixed time instant obtained from the FEA simulations with progressively decreasing element size.

Interestingly, the contours of pore pressure show that a region of strong negative pressure exists ahead of the crack tip, as shown in Fig[7-a]. Further, the magnitude of this negative pressure monotonically increases upon refining the FEA mesh. Such large negative pressure is unrealistic because, in reality, a fluid cannot sustain a negative pressure and will immediately undergo cavitation if subjected to it. Apparently, the FEA simulations without the inclusion of additional physics are unable to model cavitation of fluid when subjected to a negative pressure. Consequently, in the absence of cavitation physics, the FEA simulations essentially consider a hypothetical fluid which can sustain infinitely large negative pressure without undergoing cavitation.

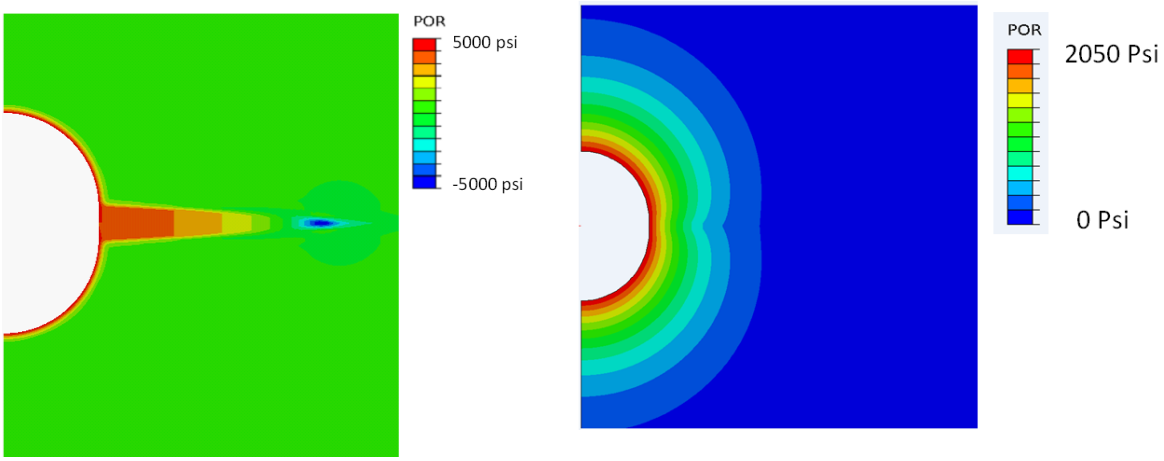

Figure 7: (a) Contour of the pore pressure in the near-tip region for formation A, showing the region of negative pore pressure ahead of the crack tip. (b) Contours of pore pressure in the near-tip region for formation B. Note the absence of a negative pore pressure for this case.

FEA simulations that involve fracture modeling based on CZM show an intrinsic mesh size dependence until the cohesive zone ahead of the crack tip is adequately resolved (Barenblatt 1959, Barenblatt 1962). Once the cohesive zone is resolved, the FEA solution becomes insensitive to the mesh size (see Fig.[8]). Does the mesh sensitivity seen in FEA simulation arise from the cohesive zone not being resolved adequately? Not really, because in such a case, the convergence is always achieved from above, i.e., the opening load decreases as the mesh size in the cohesive zone is refined further until the convergence is achieved. However, as seen in Fig.[5], in the current case, the breakdown pressure increases upon mesh refinement.

The size of the cohesive zone is given by (see Rice 1982)

$$l_{\rm cz} = \frac{9\pi}{32}\frac{G_c E}{(1-\nu^2)T_{\rm max}^2}. \tag{12}$$

where G_c is the cohesion energy, E is the interfacial stiffness, ν is the Poisson ratio, and $T_{\max}$ is the peak stress in the cohesive law used. The cohesion energy relates to the fracture toughness of the rock as follows:

$$G_c = \frac{K_{Ic}^2}{E}(1-\nu^2). \tag{13}$$

For both the formations considered in this work, the size of the cohesive zone, according to the equation (12), is obtained as $l_{cz} = 1.4$ in. However, all the element sizes considered in the mesh refinement study of this work are already sufficiently small to resolve the cohesive zone. Despite this, the simulations fail to achieve mesh convergence with continued refinement of the mesh. This suggests that the origin of the absence of the objectivity noted in this study is not related to the size of the cohesive zone.

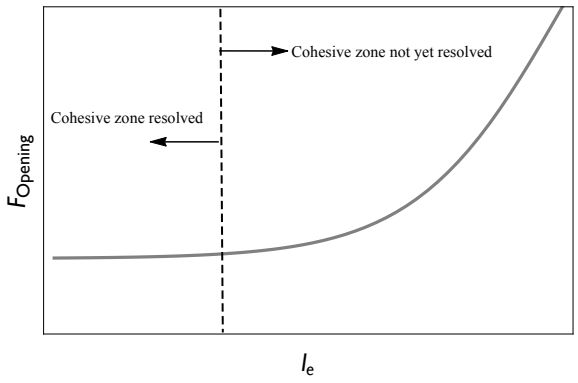

Figure 8: Schematic showing the fashion in which an FEA solution changes with mesh size when the lack of convergence is due to an unresolved cohesive zone.

3.2.2 Formation B: $k_{\text{Fluid}} = \mathcal{O}(10^{-9}\text{in/s})$

Next, a configuration is considered for which the hydraulic conductivity of the solid-fluid combination is substantially higher than that of formation A. This configuration is referred to as "Formation B" in the rest of this document. Experimentally, such a configuration is realized by combining a matrix which has an absolute permeability of $k_a = 15$ mD with a fracturing fluid which has a kinematic viscosity of $\mu = 1500$ cSt [1]. The resulting configuration has a hydraulic conductivity of $k_{\text{Fluid}} = 2.5 \times 10^{-9}$ in/s, which is 10^3 times larger than the hydraulic conductivity value of the formation A.

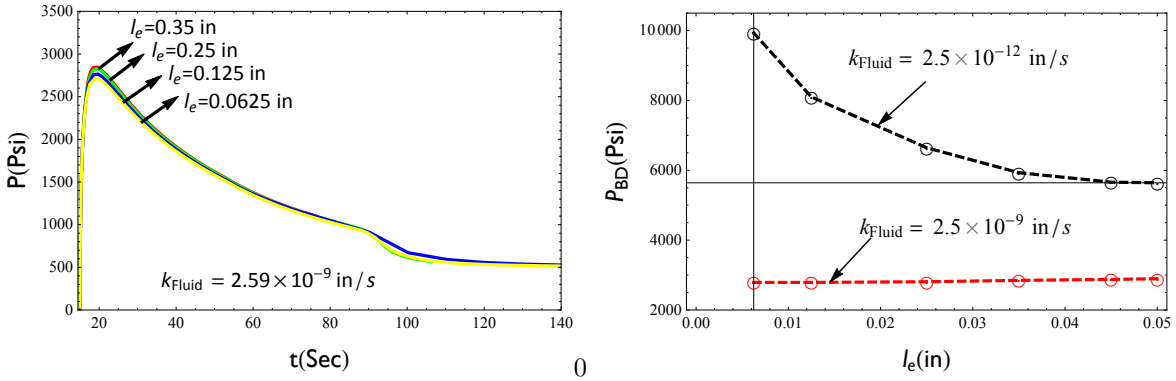

0

Figure 9: (a) Pressure response curves obtained from the FEA simulations employing different element sizes. No noticable variation in the response with variation in mesh size is seen. (b) Breakdown pressure as a function of element size for two formations. For formation B, the convergence w.r.t. element size is readily achieved while in case of formation A (ultra-low permeability configuration), the objectivity is missing.

The FEA simulation results for the case of formation B are shown in Fig.[9]. The pressure response curves obtained

[1] Note that in calculating the hydraulic conductivity, the dynamic viscosity should be used.

for different element sizes remain nearly identical (as shown in Fig.[9-a]), and the breakdown pressure vs element size curve is almost a flat line (as shown in Fig.[9-b]). Thus, unlike in the case of ultra-low k_{fluid}, the convergence w.r.t. element size in case of high k_{fluid} is readily achieved. The reason for this is that when k_{fluid} is sufficiently high, the Darcy flow allows the influx of host fluid from the surrounding medium into the region ahead of the crack tip, thus, subsiding the negative pressure build-up caused by the material dilation and regularizing the pore-pressure field. Thus, we are confronted by the following anomaly: there appears to be no *objective* FEA solution achievable for the breakdown pressure in the case of ultra-low hydraulic conductivity scenario (formation A) whereas in the relatively higher hydraulic conductivity scenario (formation B), objectivity is achieved readily.

4 Origin and resolution of lacking objectivity

4.1 Mechanistic origin

To understand the origin of lacking objectivity we note that because of an extremely low hydraulic conductivity of the solid-fluid system in formation A, there is essentially no flow of fluid through the interconnected pores of the solid in the formation. The mechanical response of the solid to an external loading under such circumstance is similar to that of a linear elastic material (and not poroelastic) with the elastic constants corresponding to the undrained solid. In what follows, we explain how such material response leads to a region of strong negative pressure ahead of the crack tip.
The material element ahead of the crack tip during the crack-opening experiences dilation, i.e., a state of biaxial tension, resulting in creation of additional pore-space (see Fig.[10]).

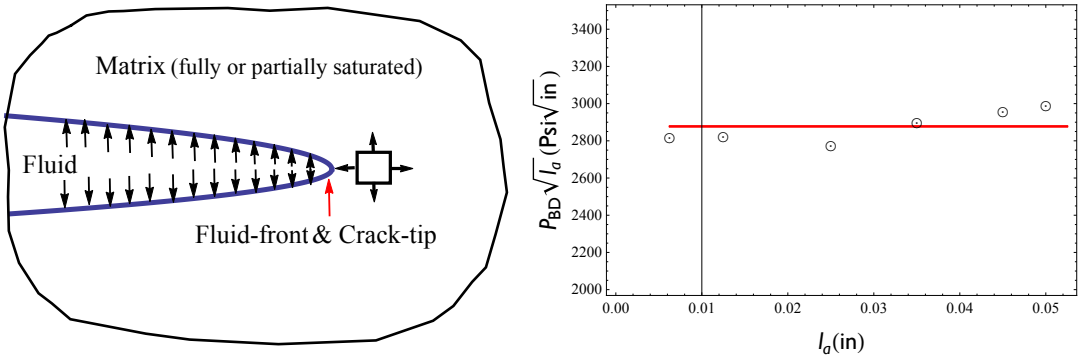

Figure 10: (a) The material element ahead of the crack tip experiences dilation during the fracture propagation. (b) $P_{BD}\sqrt{l_a}$ vs l_e indicates that the material indeed behaves like a linear elastic solid.

Had the fluid been able to flow through the material, the additional pore-space would have been immediately filled by the fluid from the surrounding medium. However, since it cannot, the dilation of the material element results in a negative pressure. In fact, for a material completely devoid of pore-fluid movement, the fracture mechanics along with the lubrication theory suggests that the pore pressure at the crack tip must show a logarithmic variation with distance x from the crack tip (Garagash 2000, Detournay 1998). This means that the pore pressure must have a negative singularity at the crack tip, i.e.,

$$p(x) \to -\infty \text{ as } x \to 0,$$

which is in agreement with the trend shown in FEA simulations which show that the pore-pressure at the crack tip approaches to large negative values upon a continued refinement of the FEA mesh. The negative singularity in the pore pressure at the crack tip may result in an infinite break-down pressure.

The effective adhesion at a crack tip is determined by J-integral, given by a contour integral of the form (Rice 1968):

$$J = \int_c \left(\psi \mathbf{n}.\hat{\mathbf{x}}_\mathbf{1} - \mathbf{t}.\frac{\partial \mathbf{u}}{\partial x_1} \right) ds, \tag{14}$$

where ψ is the elastic energy density, and $\mathbf{t}$ is the traction vector, and $\mathbf{u}$ is the displacement field. For a poroelastic material, the traction vector comprises both the material cohesion, given by the traction-separation relation, as well as the pore pressure at the crack tip. Thus, the expression for the J-integral can be simplified as follows:

$$J = \int_c (T(\Delta) - p) \frac{\partial \Delta}{\partial x_1} dx_1, \tag{15}$$

where $T(\Delta)$ is the traction-separation law, which relates the traction (T) to the separation (Δ). From equation (15), it can be readily seen that a suction will result in an enhanced adhesion between the two surfaces. Specifically, a singular negative pressure field at the crack tip would lead to a singular breakdown pressure.

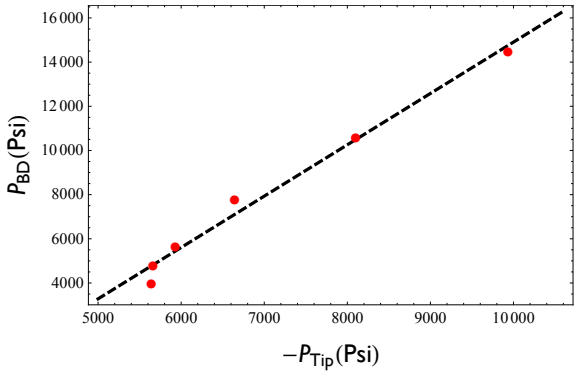

Figure 11: Breakdown pressures obtained from FEA simulations with different element sizes plotted against the corresponding pore pressure values at the crack tip P_{Tip}. Note the direct proportionality between P_{BD} and P_{Tip}, indicating that the apparent strengthening is a consequence of suction at the crack tip.

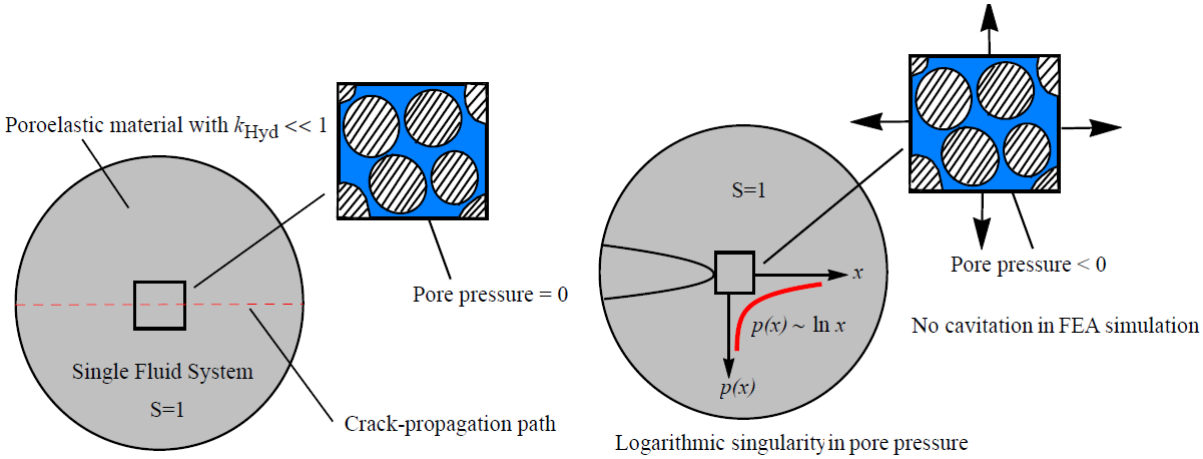

Figure 12: (a) Shown is a schematic of a rock prior to onset of fracture. The material is assumed to be fully-saturated with a uniform pore pressure. This initial pore pressure is taken as the reference value, i.e., p=0. (b) An opening crack causes dilation of the material ahead of the crack tip. As the material element ahead of the crack tip dilates, the pore pressure in the material element declines. Ordinarily, in a permeable material, in response to such declining pore pressure, the fluid from the surrounding medium would rush in to fill the extra space created and hence curbing the decline in pore-pressure. However, in a material with ultra-low permeability the conductivity of the fluid within the matrix is diminishing small, and as a result, upon continued dilation, the pore pressure in the material element tends to attain large negative values.

In reality, a fluid cannot sustain such large negative pressures, and consequently, cavitation of the fluid is bound to happen. As a result, the tip region must comprise two fluid phases: a liquid phase and a vapor phase. However, the `COD2D4P` elements in *ABAQUS* (ABAQUS 2016), as currently implemented, do not incorporate such cavitation or sorption physics in their basic element definition. Therefore, unless such physics is explicitly incorporated within the soil consolidation step, the negative pressure ahead of the crack tip cannot be alleviated.

4.2 Inclusion of cavitation and sorption

Physically, a bulk fluid cannot sustain a large negative pressure and will immediately undergo cavitation. However, a fluid which is in contact with a solid surface can sustain some negative pressure by the virtue of the surface tension without undergoing the liquid-to-vapor phase transition. Therefore, as soon as a negative pressure appears at the crack tip, the host fluid which is away from any surface instantly undergoes cavitation while the fluid in contact with the grain surface remains in the liquid phase, forming capillary bridges. Thus, the region ahead of the crack tip contains two phases of fluid: (1) the liquid state of the host fluid and (2) the vapor state of the host fluid. Let P_{liq} be the pressure of the liquid phase inside the capillary bridges while the pressure outside is simply the cavitation pressure P_{vap}, which is fixed. The pressure difference between the liquid and the vapor phases is called the capillary pressure, and is given by

$$P_c = P_{\text{liq}} - P_{\text{vap}} = -2\gamma/r_c, \tag{16}$$

where r_c is the meniscus radius associated with the capillary bridges, and γ is the surface energy associated with the liquid-vapor interface. Thus, while the cavitation pressure is fixed, the liquid pressure inside the capillary bridges varies depending upon the meniscus radius. As more and more liquid is turned into vapor, i.e., as S decreases, the meniscus radius becomes narrower and narrower, i.e. r_c decreases, and as a result the capillary pressure increases. At a continuum level, the increasing capillary pressure with decreasing saturation is modeled by means of a saturation curve, as shown in Fig.[13-a], and is implemented in *ABAQUS* using `*SORPTION` functionality within a soil consolidation step.

Capillary pressure, which is the pressure-difference across liquid-vapor interface, is the driving force for desaturation. This means that as the capillary pressure p_c gets higher and higher, the saturation of the liquid phase gets lower and lower. Post cavitation, the total pore-pressure at a given state of saturation in this region is given by

$$P(\mathcal{E}) = \chi_{\text{Liq}}\, P_{\text{liq}} + \chi_{\text{Vap}}\, P_{\text{Vap}};\ \ \chi_{\text{Liq}} + \chi_{\text{Vap}} = 1, \tag{17}$$

where $\chi_{\text{liq}} = S$ and $\chi_{\text{vap}} = 1 - S$ denote the saturation levels of the liquid and vapour phases, respectively. Continued dilation at the crack tip results in more and more evaporation of the liquid, and narrowing of the capillary bridges, i.e., r_c decreases. Recall that the suction pressure varies inversely with r_c, as evident from equation (16), thus as r_c decreases, suction of the liquid phase out of the capillary bridges due to capillary effect becomes increasingly more and more difficult.

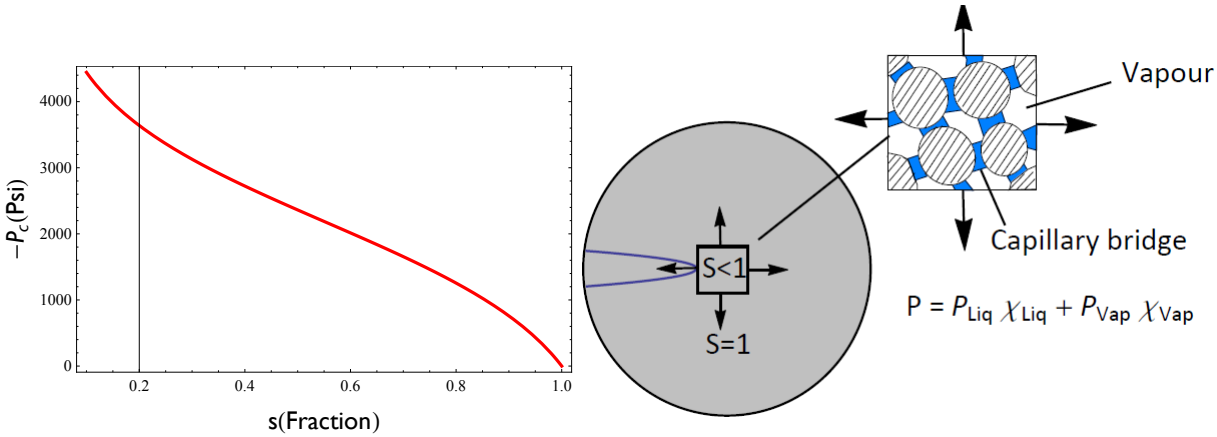

Figure 13: (a) Shown is the capillary pressure (P_c) vs saturation (S) curve employed in this work. (b) Schematic showing the crack tip region when cavitation and sorption in the material are allowed.

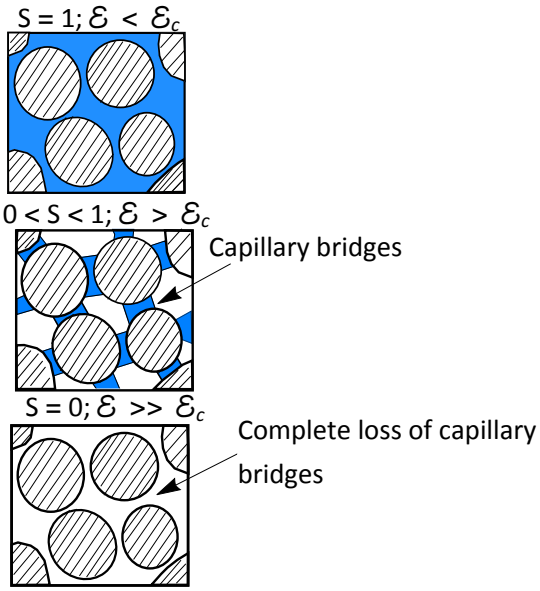

Figure 14: Mechanistic details of the cavitation and sorption-related processes at the crack tip: (a) Dilatational strain $\mathcal{E}$ at the crack tip causes expansion of pore space, subjecting the pore fluid to tension, i.e., a negative pressure. As long as the pressure remains above the cavitation pressure, pore fluid remains in the liquid state. (b) Beyond a certain critical dilatational strain, i.e., $\mathcal{E} > \mathcal{E}_c$, the pore liquid which is not in contact with a solid surface undergoes cavitation. However, liquid in the contact with the solid surface remains uncavitated due to the action of surface tension, forming capillary bridges (meniscus radius r_c). For each incremental dilation, more and more liquid cavitates, resulting in a thinning of the capillary bridges. Both the saturation of the liquid state and the meniscus radius decrease with progressive thinning of the capillary bridges. (c) Continued dilation will ultimately result in complete cavitation and eventual disappearance of the capillary bridges.

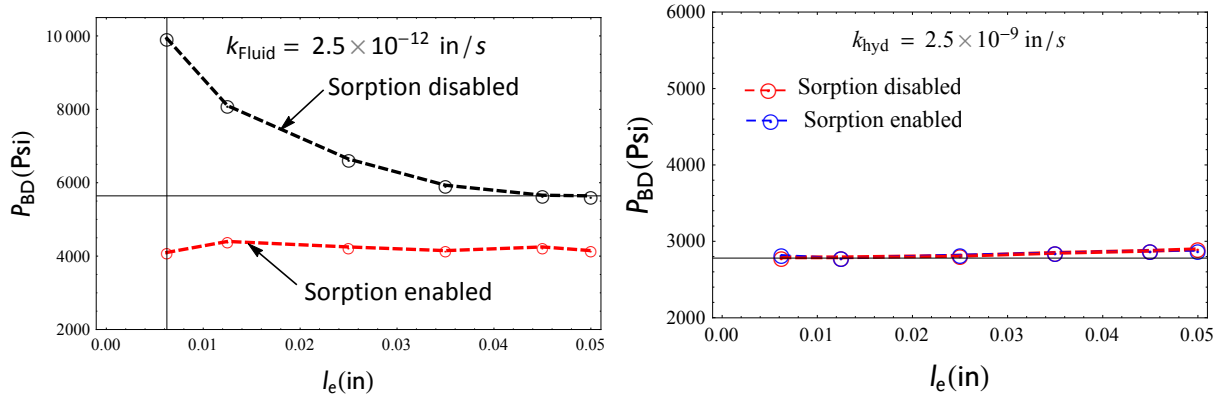

Figure 15: (a) Breakdown pressure as a function of element size with and without the sorption physics for the ultra-low permeability scenario (formation A). (b) Breakdown pressure as a function of element size with and without the sorption physics for formation B.

Fig.[15-b] shows the breakdown pressure versus element size curve with and without sorption for formation B configuration. For this case, inclusion of sorption does not make any noticeable difference in the response because in such a permeability regime, the Darcy flow between pores in response to dilation can readily occur to suppress any negative pressure that might be caused due to dilatation ahead of the crack tip.

4.3 Comparative role of Darcy flow over capillary flow: capillary number

Whether the inclusion of sorption in modeling would have a significant impact on the mechanics of hydraulic fracturing determined by the comparative role of Darcy flow over capillary flow (sorption). For example, when the hydraulic conductivity of the rock is high, the Darcy flow can readily occur to suppress any negative pressure that might be caused due to dilatation ahead of the crack tip. Sorption in such instances may not have that big of an impact on the mechanics of hydraulic fracturing. This is evident from Fig.[15-b], which shows that the response with and without sorption is essentially the same for formation B. On the other hand, when the hydraulic conductivity is ultra-low such as in the case of formation A, Darcy flow may not be sufficient to suppress the negative pressure ahead of the crack tip, and the regularization of the solution requires that cavitation and sorption behavior be incorporated in the numerical model, as seen in Fig.[15-a].

The importance of Darcy flow relative to capillary flow depends upon a number of factors including the hydraulic conductivity, the surface tension of the fluid and size of the pores in the material. The relative importance of sorption behavior over the Darcy flow is characterized by means of a dimensionless entity called the capillary number, which is defined as the ratio of viscous pressure drop to capillary pressure, i.e.,

$$C_a = \frac{\Delta p_{\text{visc}}}{\Delta p_{\text{cap}}}, \text{ where } \Delta p_{\text{visc}} \sim \frac{q\mu}{k} \text{ and } \Delta p_{\text{cap}} \sim \frac{2\gamma}{r_c}, \tag{18}$$

such that

- when $C_a >> 1$, the capillary action is relatively significant vis-à-vis Darcy flow, and its inclusion is necessary, and
- when $C_a << 1$, the mechanics is mostly dominated by Darcy flow, and inclusion of sorption may not be necessary.

5 Conclusion

Provided all necessary physics are included in a FEA simulation, the result of such a simulation should become mesh-insensitive below a certain mesh refinement. This is called objectivity, and is necessary for the solutions of the simulation to be physically realizable. If objectivity is not ensured, it will mean that the outcome of an FEA simulation can be made arbitrarily large or small simply by varying the element size, or in other words, such FEA solution will be meaningless. At a fundamental level, the absence of objectivity in an FEA simulation implies that all the necessary physics required for an adequate description of the underlying phenomena have not been accounted for in the underlying model.

By means of extensive FEA simulations, it has been shown that the FEA simulations with the existing implementation of the physical models fail in providing an objective solution for the breakdown pressure in formations with ultra-low hydraulic conductivity. Specifically, it is shown that the breakdown pressure obtained from such simulations grow without bound upon a continued refinement of the element size. Such a solution is undesirable for comparison with experiments, and if compared, it will not lead towards developing a reliable predictive capability.

This lack of objectivity has been shown to stem from the underlying model's inability to resolve the fluid cavitation and the sorption behavior in the region ahead of the crack tip. Guided by the above understanding, the cavitation and sorption physics is incorporated in the model. We show, by both explicit simulations as well as physics-based reasoning, that incorporating the sorption physics leads to regularization of the solution. Consequently, the revised FEA simulations of the PTC experiments, with cavitation and sorption physics included, provide solutions that are completely insensitive to mesh-size, and are suitable for comparison and calibration against experimentally-measured data.

The results of this work have applications in modeling of hydraulic fracturing in unconventional formations, such as shale, which have very small permeability. As noted in this work, the issue of lack of objectivity is much more of a concern in materials with ultra-low permeability. Therefore, in the absence of cavitation and sorption physics, the outcome of any FEA simulation of hydraulic fracturing in such formations, however sophisticated, would have remained questionable.

References

[1] W. El Rabaa: Hydraulic fracture propagation in the presence of stress variation. *Soc. Petro. Eng.*, 27-30 (1987).

[2] C. Terzaghi: Principles of Soil Mechanics. Engineering News-Record, **95** (19-27)(1925).

[3] M. A. Biot: General theory of three-dimensional consolidation. *J. Appl. Phys.* **12**, 155-164 (1941).

[4] J. Ning *et al.*: Experimental validation of simulation capabilities for hydraulic fractures propagating in a porous Medium. *SIMULIA Community Conference* **1**, 1-10 (2015).

[5] M. Zielonka *et al.*: Development and validation of fully-coupled hydraulic fracturing simulation capabilities. *SIMULIA Community Conference* **1**, 1-31 (2014)

[6] M. A. Biot: Theory of elasticity and consolidation for a porous anisotropic solid.*J. Appl. Phys.* **26**, 182-185 (1955).

[7] M. A. Biot: General solutions of the equations of elasticity and consolidation for a porous material. *J. Appl. Mech.* **78**, 91-96 (1956).

[8] D. Garagash, and E. Detournay: The tip region of a fluid-driven fracture in an elastic medium.*J. App. Mech.* **67**,183-192 (2000).

[9] D. S. Dugdale: Yielding of steel sheets containing slits. *J. Mech. Phys. Solids* **8**,100-104 (1960).

[10] G. I. Barenblatt: The formation of equilibrium cracks during brittle fracture: general ideas and hypothesis, axially symmetric cracks. *J. Appl. Math. Mech.* **23**, 622-636 (1959).

[11] G. I. Barenblatt: The mathematical theory of equilibrium cracks in brittle fracture. *Advances in Applied Mechanics* (Academic Press, New York (1962)).

[12] D. Garagash, and E. Detournay: The tip region of a hydraulic fracture propagating in a permeable rock. Poromechanics II, 77-94 (2000).

[13] E. Detournay, and A. H-D. Cheng: Poroelastic response of a borehole in a non-hydrostatic stress field. *Int. J. Rock Mech.* **25**, 171-182 (1988).

[14] M. S. Bruno, and F. M. Nakagawa: Pore pressure influence on tensile fracture propagation in sedimentary rock. *Int. J. Rock Mech.* **28**, 261-273 (1991).

[15] D. R. Schmitt, and M. D. Zoback: Poroelastic effects in the determination of the maximum horizontal principal stress in hydraulic fracturing tests- a proposed breakdown equation employing a modified effective stress relation for tensile failure. *Int. J. Rock Mech.* **26**, 499-506(1989).

[16] A. M. Rubin: Tensile fracture of rock at high confining pressure: implications for dike propagation. *J. Geophys. Res.* **89**, 919-935 (1993).

[17] J. S. Y. Wang, and T. N. Narasimhan: Hydrologic mechanisms governing fluid flow in a partially saturated, fractured, porous medium. *Wat. Res. Res.* **21**, 1861-1874 (1985).

[18] G. Lovoll, Y. Méheust, K. J. Maloy, E. Aker, and J. Schmittbuhl: Competition of gravity, capillary and viscous forces during drainage in a two-dimensional porous medium, a poro-scale study. *Energy* **30** 861-872 (2005).

[19] J. C. Jaeger, N. G. W. Cook, and R. W. Zimmerman: *Fundamentals of Rock Mechanics* (Fourth edition, Blackwell Publishing, Oxford, UK(2007)).

[20] J. R. Rice, A path independent integral and the approximate analysis of strain concentration by notches and cracks. J. Appl. Mech. 379-386 (1968).

[21] M. D. Zoback: *Reservoir Geomechanics* (First edition, Cambridge University Press, Cambridge (UK) 2007).

[22] *ABAQUS/STANDARD*, Dassault Systemes Simulia 2016.